

Excitation of Central Nervous System Neurons by Nonuniform Electric Fields

Cameron C. McIntyre and Warren M. Grill

Department of Biomedical Engineering, Case Western Reserve University, Cleveland, Ohio 44106-4912 USA

ABSTRACT The goal of this study was to determine which neural elements are excited by microstimulation of the central nervous system. A cable model of a neuron including an axon, initial segment, axon hillock, soma, and simplified dendritic tree was used to study excitation with an extracellular point source electrode. The model reproduced a wide range of experimentally documented extracellular excitation patterns. The site of action potential initiation (API) was a function of the electrode position, stimulus duration, and stimulus polarity. The axon or initial segment was always the site of API at threshold. When the electrode was positioned near the cell body, the site of excitation was dependent on the stimulus amplitude. With the electrode in close proximity to the neuron, short-duration cathodic pulses produced lower thresholds with the electrode positioned over the axon than over the cell body, and long-duration stimuli produced opposite relative thresholds. This result was robust to alterations in either the maximum conductances or the intracellular resistivities of the model. The site of maximum depolarization was not always an accurate predictor of the site of API, and the temporal evolution of the changes in membrane potential played a strong role in determining the site of excitation.

INTRODUCTION

Electrical stimulation of the central nervous system (CNS), both clinically and experimentally, has led to a wide range of benefits for individuals with impairments and the exploration of a variety of physiological phenomena. However, little is known about the cells or cell elements that are activated by electrical stimulation of the CNS (Gustafsson and Jankowska, 1976; Norwak and Bullier, 1998a,b). In microstimulation of the CNS, the stimulating electrode is placed within an electrically and geometrically complex volume conductor containing cell bodies, dendrites, and axons in close proximity. When a stimulus is applied within the CNS, cells and fibers over an unknown volume of tissue are activated (Ranck, 1975). To make accurate inferences about anatomical structures or physiological mechanisms involved in electrical stimulation, one must know which elements are stimulated. The goal of the present study was to determine which neural elements are excited by microstimulation of the CNS and how the initial site of activation varies with electrode location, stimulus duration, and stimulus polarity.

This study used a computer model as an analytic tool to study the controlled activation of neurons with extracellular sources. This approach enabled us to examine the influence of various parameters on excitation under controlled conditions that would be extremely difficult to achieve experimentally. The model structure was based on the documented physiological characteristics of cat somatic

motoneurons (Schwindt and Crill, 1984; Cullheim et al., 1987; Fleshman et al., 1988; Clements and Redman, 1989). The motoneuron was selected from the wide range of cell types in the CNS because of the body of data available to parameterize the model and previous single-cell mapping experiments, to which model results could be compared (Gustafsson and Jankowska, 1976).

This study addresses the fundamental issue of how electric fields, generated by the passage of current through the extracellular space, affect the excitation of geometrically complex neurons. The solution to this problem depends on the relationship between the orientation of the applied field and the geometry of the neuron. Tranchina and Nicholson (1986) modeled a passive neuron stimulated by a uniform electric field and demonstrated that the neural geometry is a crucial factor in determining the response to applied electric fields and that the soma would be the likely site of action potential initiation. The present study is an extension of that work that incorporates an active model in combination with a nonuniform electric field (generated by a point source electrode). The results show that excitation at threshold always occurred in the initial segment or the axon, rather than the cell body. Furthermore, the site of maximum depolarization was not an accurate predictor of the site of excitation, as suggested previously (Rattay, 1998), and the temporal evolution of the changes in membrane potential played a strong role in determining the site of action potential initiation. Preliminary portions of this work have been presented as an abstract (McIntyre and Grill, 1997).

METHODS

A computer-based cable model of a spinal motoneuron was used to study the excitation of CNS neurons with an extracellular point-source electrode. The model morphology included 20 nodes of a myelinated axon, an initial segment, an

Received for publication 19 August 1998 and in final form 22 September 1998.

Address reprint requests to Dr. Warren M. Grill, Applied Neural Control Lab, Case Western Reserve University, C.B. Bolton Building, Rm. 3480, Cleveland, OH 44106-4912. Tel.: 216-368-8625; Fax: 216-368-4872; E-mail: wmg@po.cwru.edu.

© 1999 by the Biophysical Society

0006-3495/99/02/878/11 \$2.00

axon hillock, a three-compartment soma, and a tapering dendritic structure (Fig. 1, Table 1). The neuron was represented by equivalent electrical circuits with elements representing the membrane, transmembrane ion channels, and the ionic Nernst potentials. The electrical parameters of the model are given in Table 2. The cytoplasmic resistivity of the cell body was set to a value greater than that of the axon to facilitate somatic invasion of antidromic action potentials (Traub et al., 1994).

The geometric profile of the equivalent dendritic cable was a uniform cylinder for 0.5λ (where λ is the dendritic length constant; $\lambda = 2800 \mu\text{m}$) and thereafter was tapered to a final termination at 2λ from the soma (Clements and Redman, 1989). From the $3/2$ power constraint of Rall (1977), a stem diameter of $25 \mu\text{m}$ with a branching of 2 was used for the cylinder representing the dendritic tree. The length of each dendritic compartment was constructed such that all compartments had an electrotonic length of $<0.2\lambda$ (Segev et al., 1985).

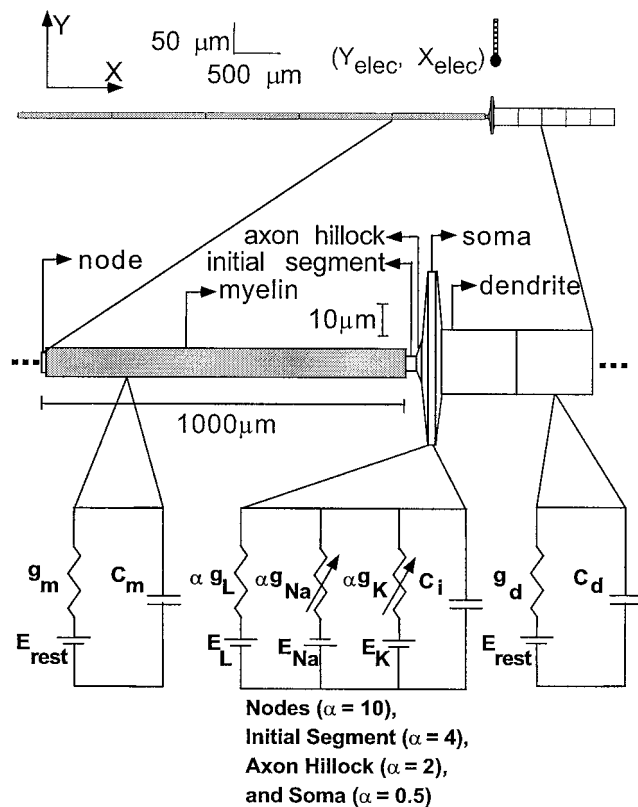


FIGURE 1 Morphology and membrane models of a cable model of a spinal motoneuron. The model consisted of a myelinated axon with 20 nodes separated by 20 myelin internodes with an internodal spacing of $1000 \mu\text{m}$. The cell body of the model included an initial segment, axon hillock, three-compartment soma, and tapering dendrite. The model was stimulated by an extracellular point source electrode that could be placed in any position around the neural structure to study the effects of electrode position on excitation. The myelin internodes and dendrite used passive membrane dynamics. The node, initial segment, axon hillock, and soma compartments used Hodgkin-Huxley membrane dynamics with scaled (α) maximum conductances.

The model used two types of membrane dynamics (Fig. 1). The myelin internode and the dendritic sections were modeled with linear membrane dynamics consisting of the parallel combination of a linear conductance and membrane capacitance. The nodes of the axon and the sections of the cell body (initial segment, axon hillock, and soma) were modeled with nonlinear membrane dynamics consisting of the parallel combination of a nonlinear sodium conductance, a nonlinear potassium conductance, a linear leakage conductance, and a membrane capacitance (Fig. 1). The nonlinear conductance properties were originally obtained from experimental data from squid giant axons (Hodgkin and Huxley, 1952), and thus the maximum conductances of each active section were scaled to approximate the firing properties of cat spinal motoneurons. The maximum conductances of the fast sodium, fast potassium, and leakage channels were scaled by factors of 10, 4, 2, and 0.5 for the node, initial segment, axon hillock, and soma, respectively (Hines and Moore, 1991).

The model was stimulated with an extracellular point-source electrode within an infinite homogeneous medium. The electrode was placed at a position X_{elec} along and Y_{elec} above the neural structure (Fig. 1). The value of the extracellular potential, $V(n)$, at each segment, $\{X(n), Y(n)\}$, was determined by

$$V(n) = I_{\text{ext}}\rho_{\text{ext}}/[4\pi\{(X(n) - X_{\text{elec}}) + (Y(n) - Y_{\text{elec}})\}^{1/2}] \quad (1)$$

where I_{ext} was the amplitude of the extracellular current pulse and ρ_{ext} was the extracellular resistivity (Warman et al., 1992). With the extracellular potential calculated for each individual segment of the model, an equivalent set of intracellular current sources were calculated and then used to stimulate the neuron. The magnitudes of these equivalent intracellular currents, $I_{\text{int}}(n)$, were described at each segment, n , by

$$I_{\text{int}}(n) = G_i(-)[V(n-1) - V(n)] + G_i(+)[V(n+1) - V(n)] \quad (2)$$

where $G_i(-)$ represents the intersegmental conductance between the n and $n-1$ compartments and $G_i(+)$ represents the intersegmental conductance between the n and $n+1$ compartments of the model (Warman et al., 1992). If $G_i(-) = G_i(+)$, then Equation 2 reduces to

$$I_{\text{int}}(n) = G_i[V(n-1) - 2V(n) + V(n+1)] \quad (3)$$

The transmembrane voltage response at each compartment of the cable, $V_m(n, t)$, in response to the applied equivalent intracellular currents, $I_{\text{int}}(n)$, was calculated by numerical integration of the nonlinear differential equation:

$$C_m(n)[dV_m(n, t)/dt] + G_m(V_m, n, t)V_m(n, t) - G_i[V_m(n-1) - 2V_m(n) + V_m(n+1)] = I_{\text{int}}(n) \quad (4)$$

where the membrane conductance, $G_m(V_m, n, t)$, which includes all ionic conductances, and the membrane capaci-

TABLE 1 Model morphology

Neural element	Diameter (μm)	Length (μm)	No. [§]	Reference
Axon node	7	1.5	1	Fabricsius et al. (1994)
Myelin internode	10	998.5	5	Fabricsius et al. (1994)
Initial segment	4	30	1	Cullheim and Kellerth (1978)
Axon hillock	4:20*	15	1	Kellerth et al. (1979)
Soma1	20:60*	20	1	Cullheim et al. (1987)
				Fleshmen et al. (1988)
Soma2	60	20	1	Cullheim et al. (1987)
				Fleshmen et al. (1988)
Soma3	60:25 [#]	20	1	Cullheim et al. (1987)
				Fleshmen et al. (1988)
Dendrite cylinder	25	1400	5	Cullheim et al. (1987)
				Fleshmen et al. (1988)
Dendrite taper	25:0.6 [#]	4200	15	Clements and Redman (1988)

*Linear increase from initial diameter to final diameter.

[#]Linear decrease from initial diameter to final diameter.

[§]Number of compartments representing the given neural element.

tance, $C_m(n)$, are dependent on n to indicate that they vary in the different elements of the neuron.

All model simulations were run using the NEURON simulation package (Hines, 1993; Hines and Carnevale, 1997). The Crank-Nicholson (C-N) implicit integration method was used with a time step of 0.001 ms. This method, which is accurate for small time steps, has a numerical error proportional to Δt^2 . The threshold stimulus calculated using a time step of 0.001 ms was within 1% of the threshold stimulus calculated using a time step of 0.0001 ms, and a step of 0.001 ms was used for subsequent simulations. Threshold currents needed to generate a propagating action potential with monophasic rectangular pulses were calculated to within 1%, for a range of electrode positions and stimulus pulse durations (0.01–2.0 ms).

RESULTS

Threshold profile along the neural structure

Profiles of the threshold current were calculated at 50- μm increments along the longitudinal axis (x) of the neuron with vertical distances of the electrode above the neuron (y) of 50, 100, 250, and 500 μm . These profiles were generated with monophasic rectangular anodic and cathodic stimuli over a range of stimulus pulse durations (0.01–2.0 ms). Fig.

2 shows examples of these threshold profiles for the four electrode-to-neuron distances with a 0.1-ms stimulus pulse duration.

With the electrode positioned over the axon, a sinusoidal pattern in the magnitude of the threshold current was found, using both cathodic and anodic stimulus pulses, with minima over the nodes and maxima over the middle of the myelin internodes. The relative difference in the peak-to-peak amplitude of the sinusoidal pattern was greater for small (50 μm) compared to large (500 μm) electrode-to-neuron distances. The ratio of the anodic pulse to the cathodic pulse threshold current ranged from 4.02 (electrode over the middle of a myelin internode) to 6.15 (electrode over an axon node).

For both cathodic and anodic stimuli, the threshold current increased as the electrode-to-neuron distances increased. With cathodic stimuli the increase in threshold current due to the increase in the electrode-to-neuron distance was larger for electrode positions over the cell body than for electrode positions over an axon node (Fig. 2 A). This trend was the opposite for anodic stimuli; the increase in threshold current due to the increase in the electrode-to-neuron distance was smaller for electrode positions over the cell body than for electrode positions over an axon node (Fig. 2 B). With the electrode over the area of the cell body

TABLE 2 Model electrical parameters

Parameter	Value	Reference
Neuron resting potential (E_{rest})	-70 mV	
Extracellular resistivity (ρ_{ext})	300 $\Omega\text{-cm}$	
Intracellular resistivity		
Axon fiber (ρ_{axon})	60 $\Omega\text{-cm}$	Barrett and Crill (1974)
Cell body, dendrite (ρ_{CB})	300 $\Omega\text{-cm}$	Thurbon et al. (1998)
Membrane capacitance (C_i)	1 $\mu\text{F}/\text{cm}^2$	Fleshmen et al. (1988)
Dendrite membrane capacitance (C_d)	1 $\mu\text{F}/\text{cm}^2$	Fleshmen et al. (1988)
Dendrite membrane conductance (g_d)	0.0003 S/cm ²	Thurbon et al. (1998)
Myelin membrane capacitance (C_m)	0.005 $\mu\text{F}/\text{cm}^2$	Tasaki (1955)
Myelin membrane conductance (g_m)	0.000015 S/cm ²	Stephanova and Bostock (1995)

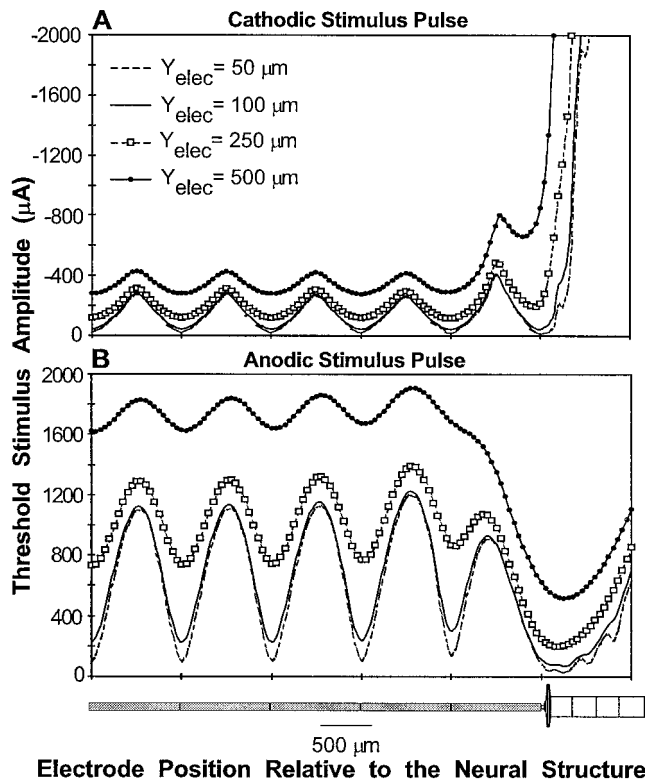


FIGURE 2 Threshold profiles for electrode-to-neuron distances of 50, 100, 250, 500 μm and a stimulus pulse duration of 0.1 ms. The plots show the threshold profiles for cathodic (A) and anodic (B) stimulation. The electrode was positioned radially from the central axis of the neuron, and the threshold needed to generate a propagating action potential was calculated ($\pm 1\%$) at 50- μm intervals along the longitudinal axis of the neural structure.

there was a shift in the local minimum for cathodic stimuli from over the initial segment, for small electrode-to-neuron distances, to the first myelin internode 200 μm from the initial segment for large electrode-to-neuron distances. In the case of anodic stimuli, this shift moved in the opposite direction; at small electrode-to-neuron distances the local minimum was over the cell body, and at larger electrode-to-neuron distances the minimum was over the dendrite, 350 μm from the cell body. The ratio of the anodic pulse to the cathodic pulse threshold current ranged from 0.92 to 0.38 (decreasing with increasing electrode-to-neuron distance) with the electrode over the cell body.

For both anodic and cathodic stimuli, as the electrode moved over the dendrite, the threshold rose as the lateral distance from the cell body increased. Action potentials could not be initiated in the dendrite, and therefore the active compartments of the cell had to be stimulated. The ratio of the anodic pulse to the cathodic pulse threshold current ranged from 0.36 to 0.04 (decreasing with increasing distance from the cell body) with the electrode over the cell body. The fluctuations in threshold at small electrode-to-neuron distances indicate switching in the element of action potential initiation from the axon, to the initial segment, to the axon hillock (see below, Fig. 5).

Site of action potential initiation

The major questions of this study were: what neural elements are excited by extracellular microstimulation and how does changing stimulus parameters alter the site of action potential (AP) initiation for a given electrode position relative to the neural structure? Figs. 3 and 4 show AP initiation and propagation, using 0.1-ms-duration cathodic and anodic stimulus pulses at four different electrode positions along the longitudinal axis of the neuron at an electrode-to-neuron distance of 100 μm .

The site of AP initiation was determined from the transmembrane voltage of the individual neural elements. The scaling of the maximum conductances of the individual model elements caused the upstroke of the AP for the cell body components to be slower than that of the nodes. Therefore, the time to peak of the AP was less for a node than for the soma. To compare the site of AP initiation and not be biased toward the node, the element that reached a membrane potential of +30 mV relative to the rest potential first, after the initial stimulus artifact, was deemed the element where the AP was initiated. The value of +30 mV relative to rest potential was chosen because it was slightly larger than the threshold transmembrane potential.

For a cathodic stimulus applied away from the cell body, the node closest to the electrode was always the site of AP

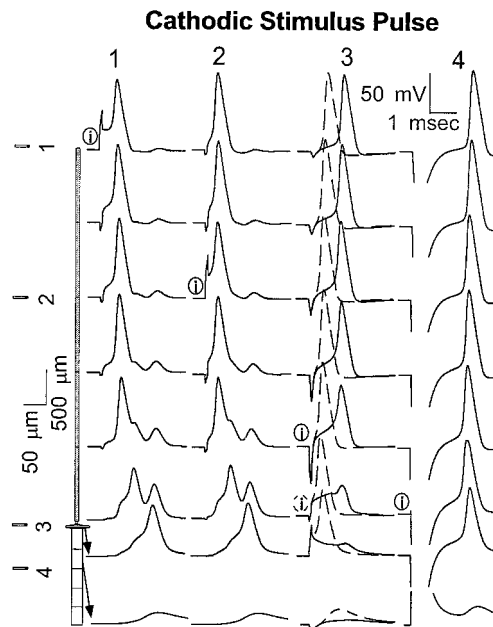


FIGURE 3 Action potential initiation (API) and propagation for four different electrode locations (electrode-to-neuron distance of 100 μm) and cathodic stimulus pulses with durations of 0.1 ms. Each column corresponds to the electrode position (1, 2, 3, or 4), and each row shows the transmembrane voltage as a function of time at the segment of the neuron shown to the left. The solid traces are responses to threshold current, and the dashed lines are responses to 110% of threshold current. The site of API is noted by the circled i, with the solid circle indicating the site of API at threshold and the dashed circle indicating the site of API at the 110% threshold. For electrode position 4 the site of API did not change from the initial segment at 110% of threshold current.

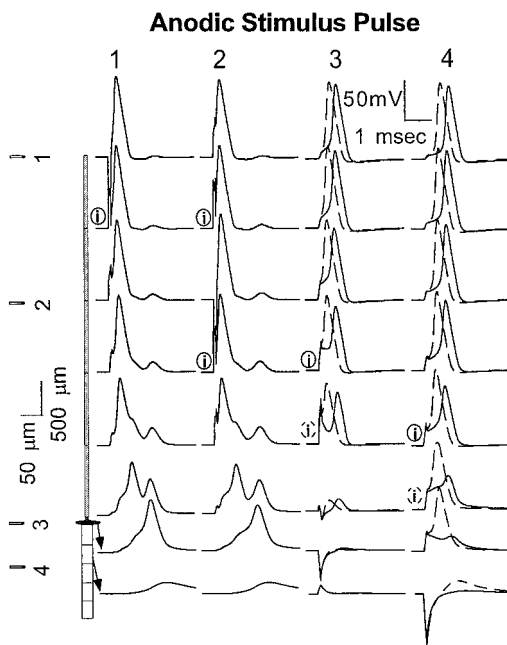


FIGURE 4 Action potential initiation (API) and propagation for four different electrode locations (electrode-to-neuron distance of $100\ \mu\text{m}$) and anodic stimulus pulses with durations of $0.1\ \text{ms}$. Each column corresponds to the electrode position (1, 2, 3, or 4), and each row shows the transmembrane voltage as a function of time at the segment of the neuron shown to the left. The solid traces are responses to threshold current, and the dashed lines are responses to 110% of threshold current. The site of API is noted by the circled *i*, with the solid circle indicating the site of API at threshold and the dashed circle indicating the site of API at the 110% threshold.

initiation (Fig. 3, electrode positions 1 and 2). The antidromic APs generated from electrode positions 1 or 2 invaded the initial segment and soma. Once the initial segment and soma reached threshold and fired APs, they individually produced nonpropagating orthodromic responses, resulting in the second and third phases of depolarization in the nodal transmembrane potential near the cell body (Fig. 3). If the electrode was positioned over the cell body (Fig. 3, position 3), the first node of the axon distal to the soma was the site of AP initiation at threshold. The depolarization of the cell body was not large enough to generate an action potential, but contributed to the repolarization of the first node after the period of hyperpolarization during the stimulus. The response of the axon node was not the result of anode break excitation. Intracellular stimulation at the first node of the axon with hyperpolarizing pulse durations less than $0.2\ \text{ms}$ were unable to excite the neuron. At longer pulse widths, intracellular stimulation at a single compartment could generate anode break excitation, but the magnitude of the hyperpolarization needed to generate an action potential was much greater than the initial hyperpolarization an element experienced by threshold extracellular stimulation. The hyperpolarization released the inactivation of the sodium channels, and the depolarizing influence of the cell body acted to repolarize the first node past threshold to initiate an AP. If the stimulus amplitude was increased to

110% of threshold at the same electrode position, the site of AP initiation switched from the first node of the axon to the initial segment (Fig. 3, position 3, *dashed traces*). With the extracellular current equal to 110% of threshold, the depolarization of the initial segment became suprathreshold before the first node of the axon recovered from hyperpolarization. If the electrode was placed over the dendrite (Fig. 3, position 4), all of the excitable sections of the model were hyperpolarized during the stimulus. The initial segment became the site of AP initiation because of a release of inactivation of the sodium channels and the depolarizing influence from the dendrites. Thus, for electrodes not positioned over the axon, the temporal evolution of the transmembrane potential, rather than the point of maximum depolarization during the stimulus, determined the site of AP initiation.

For an anodic stimulus delivered over the axon far from the cell body, the two nodes adjacent to the node under the electrode were the sites of simultaneous AP initiation (Fig. 4, positions 1 and 2). As with cathodic stimulation, antidromic APs invaded the initial segment and soma and resulted in nonpropagating orthodromic responses. With the electrode positioned over the cell body (Fig. 4, position 3), the AP was initiated in the second node distal to the soma. The first node was depolarized, but not sufficiently to initiate an AP because of the strong hyperpolarization of the adjacent cell body. The second node was depolarized by the stimulus (to a lesser degree than the first node, but both of the compartments adjacent to the second node were also depolarized), and the AP was initiated here after cessation of the stimulus. When the stimulus amplitude was increased to 110% of threshold, the site of AP initiation switched from the second node to the first node distal to the soma. The depolarizing current from the stimulus pulse was sufficient to generate an AP in the first node, even with the hyperpolarizing contribution of the cell body. When the electrode was positioned over the dendrite (Fig. 4, position 4), the site of AP initiation at threshold was the first node. When the stimulus amplitude was increased to 110% of threshold, the site of AP initiation switched from the first node to the initial segment. These results demonstrate that the site of AP initiation was dependent on the position of the electrode and the polarity and amplitude of the stimulus. Furthermore, the location of the maximum depolarization was not always the site of AP initiation, and in no case was the AP initiated in the soma with stimulus current amplitudes near threshold.

To examine the effects of the electrode-to-neuron distance on the site of action potential initiation, current-distance relationships (CDRs) were generated with the electrode placed over a node of Ranvier far from the cell body and with the electrode placed over the cell body, using cathodic stimuli of various durations. Fig. 5 *A* shows the CDRs with a 0.1-ms stimulus pulse duration, and Fig. 5 *B* shows the CDRs with a 1.0-ms stimulus pulse duration. For all electrode-to-neuron distances and both the 0.1-ms and 1.0-ms stimulus durations, the site of AP initiation with the electrode positioned over the axon was always in the node

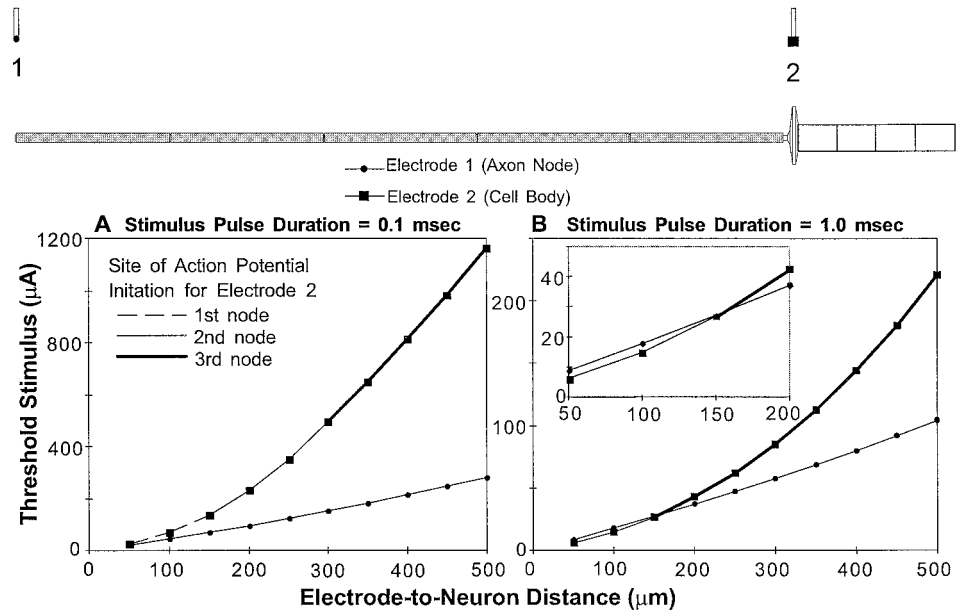


FIGURE 5 Current-distance relationships with the electrode positioned over the node (electrode position 1) and soma (electrode position 2) for stimulus pulse durations of 0.1 ms (A) and 1.0 ms (B). The site of action potential initiation for electrode positions over the soma is given by the different line types.

closest to the electrode. With a stimulus pulse duration of 0.1 ms, the site of AP initiation with the electrode over the cell body was the first node distal to the soma for small electrode-to-neuron distances (50–150 μm), then switched to the second node distal to the soma for a range of 150–300 μm , and finally switched to the third node distal to the soma for the remainder of the distances examined (300–500 μm) (Fig. 5 A). With a stimulus pulse duration of 1.0 ms (Fig. 5 B), the site of AP initiation was the second node distal to the soma for small electrode-to-neuron distances (50–150 μm), and then switched to the third node distal to the soma for the remainder of the distances examined (150–500 μm). For small electrode-to-element distances (50–150 μm) and long stimulus pulse durations (1.0 ms), less current was required

to excite the neuron with the electrode positioned over the cell body than with the electrode positioned over the axon (Fig. 5 B).

Comparison of the activation of one cell over another with the same electrode

To study the stimulation of different neural elements, excitation of two different neurons in different positions equidistant from the electrode was compared. The electrode was positioned over the cell body of one neuron (cell 1) and over an axon node of the other neuron (cell 2). Fig. 6 shows the normalized difference between the threshold for activation

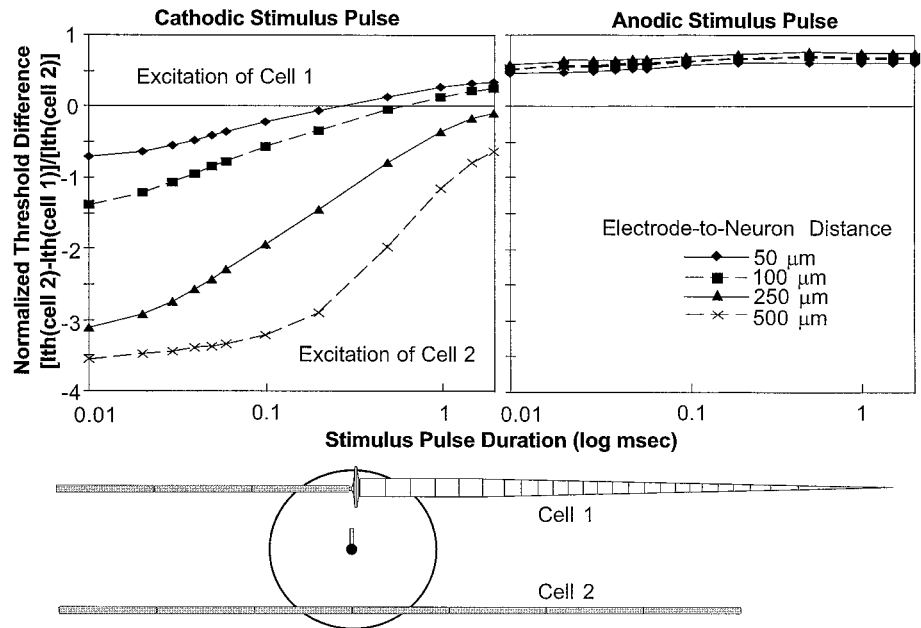


FIGURE 6 The normalized threshold difference between two neurons (cell 1 and cell 2) as a function of stimulus duration for electrode-to-neuron distances of 50, 100, 250, and 500 μm . The electrode, equidistant from both neurons, was positioned over the cell body of one neuron (cell 1) and over an axon node of the other neuron (cell 2). When the value of the normalized threshold difference was positive, cell 1 was stimulated with less current, whereas if the normalized threshold difference was negative, cell 2 was stimulated with less current. Normalized threshold difference values of 0 mark stimulus parameters and electrode positions where the thresholds of cell 1 and cell 2 were equal.

of cell 2 and the threshold for activation of cell 1 as a function of the stimulus pulse duration for cathodic and anodic stimulus pulses. With a cathodic stimulus and the electrode in close proximity to the neurons, either cell could be stimulated with less current than the other by varying the duration of the stimulus. Less current was required to excite cell 2 (axon) with short stimulus durations (<0.5 ms), whereas cell 1 had lower thresholds with larger duration stimuli. With the electrode at greater distances from the neurons (electrode-to-element distances of 250 and 500 μm), less current was required to excite cell 2 than cell 1 over the entire range of stimulus pulse durations. In the case of an anodic stimulus pulse, cell 1 was excited with less current than cell 2 at all electrode-to-neuron distances over the entire range of stimulus pulse durations. These results demonstrate that which neural elements were excited was dependent on the duration and polarity of the stimulus.

Sensitivity of the "cell 2/cell 1 threshold difference" to model parameters

A sensitivity analysis was conducted to examine the robustness of the threshold difference between different neural elements to changes in model parameters. Two primary parameters of the model, the scaling factors used for the maximum conductances and the cytoplasmic resistivities of the individual segments of the model, were varied, and the normalized cathodic threshold difference between neurons 1 and 2 was determined. The maximum conductances in each segment were originally set to reproduce the firing behavior of mammalian motoneurons (Hines and Moore, 1991). The cytoplasmic resistivities of the axon, cell body, and dendrite were selected based on experimental values and to enable antidromic invasion of the action potential into the soma.

A sensitivity analysis was conducted to determine the effect of doubling or halving the maximum conductances (g_{max}) of the individual sections of the model (Fig. 7). Doubling the g_{max} of the node resulted in only small changes in the normalized threshold difference toward excitation of cell 2 (axon). The normalized threshold difference was more sensitive to decreases in the g_{max} of the node; halving it caused a shift at all electrode-to-neuron distances toward excitation of cell 1 (cell body) and inversion of the normalized threshold difference at short stimulus pulse durations. Halving the g_{max} of the node also resulted in an inability to generate propagating action potentials in cell 2 (axon) with long stimulus pulse durations due to anodal surround block (demarcated region in Fig. 7). Increasing the g_{max} of the initial segment caused a shift in the normalized threshold difference toward excitation of cell 1, whereas decreasing the g_{max} of the initial segment had little effect. Increasing the g_{max} of the soma caused a shift in the normalized threshold difference toward excitation of cell 1, whereas decreasing the g_{max} of the soma had little effect.

In the light of recent findings indicating that the density of sodium channels in the initial segment is similar to that in

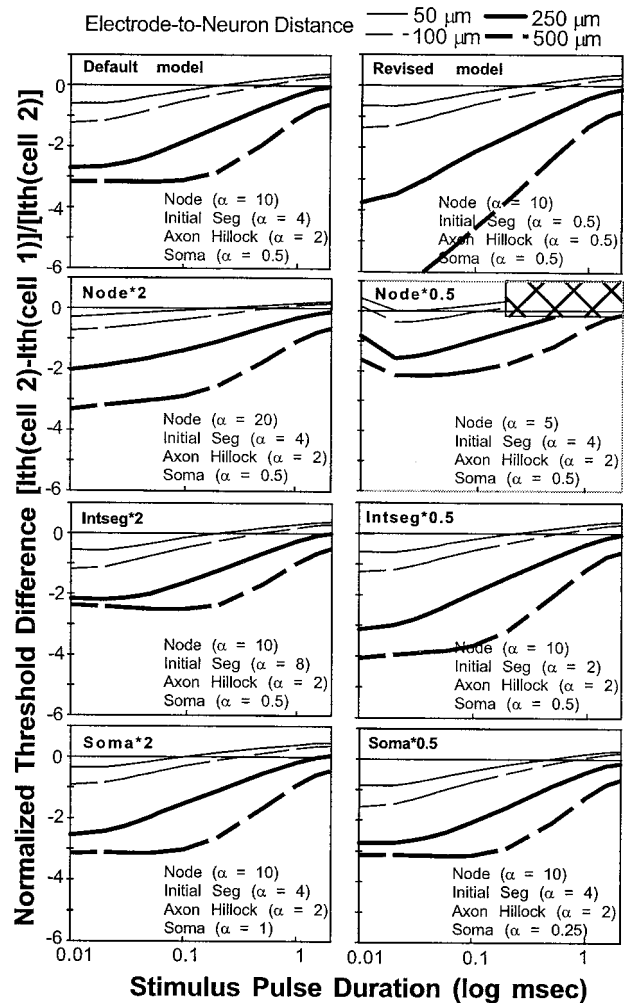


FIGURE 7 Sensitivity of the normalized threshold differences to changes in the maximum conductances (g_{max}). The g_{max} of the node, initial segment (intseg), and soma were all doubled and halved individually. A revised model was also examined with equal g_{max} for each of the cell body components.

the soma (Colbert and Johnson, 1996), a revised model with equal density of sodium channels in each of the cell body elements and a sodium channel density of the axon node 20 times that of the cell body (Hille, 1992; Mainen et al., 1995) was generated. The normalized threshold difference between cell 1 (cell body) and cell 2 (axon) for this model was very similar to that of the default model, but showed a shift toward excitation of cell 2 at large electrode-to-neuron distances and short stimulus pulse durations. These results demonstrate that the conclusions about which neural elements are excited by microstimulation (Fig. 6) were robust to relatively large changes in the conductance properties of the model neurons.

A sensitivity analysis was also conducted to determine the effect of the cytoplasmic resistivities on the threshold difference between the two neighboring neurons. The cytoplasmic resistivities of the axon segments and the cell body segments were individually doubled and halved, and models

with all intracellular resistivities equal to 100 and 300 Ω -cm were examined (Fig. 8). The value of cytoplasmic resistivities in mammalian neurons is uncertain (Rall et al., 1992), and experimentally measured values of the cytoplasmic resistivity vary from 50 to 400 Ω -cm (Barrett and Crill, 1974; Thurbon et al., 1998). Alterations in the intracellular resistivities generated, in some cases, models that failed to exhibit antidromic invasion of the soma (Fig. 8). Increasing the axoplasmic resistivity caused very little change in the normalized threshold difference, whereas decreasing the axoplasmic resistivity resulted in a shift, at all electrode-to-neuron distances, toward excitation of cell 1 (cell body) and inversion of the normalized threshold difference curves at short stimulus durations. Increasing the intracellular resistivity of the cell body components caused a decrease in the threshold difference between cell 2 (axon) and cell 1 at

larger electrode-to-neuron distances (250–500 μ m), but had little effect at smaller electrode-to-neuron distances (50–100 μ m). Decreasing the intracellular resistivity of the cell body resulted in a slight shift toward excitation of cell 1 at all electrode-to-neuron distances. With resistivity values equal for all elements of the model, decreasing the intracellular resistivity led to a decrease in the absolute differences between excitation of cell 2 over cell 1; however, there was no antidromic action potential invasion of the cell body. These results demonstrate that the conclusions regarding which neural elements are excited by microstimulation (Fig. 6) were robust to changes in the intracellular resistivity values used in the model.

DISCUSSION

The goal of this study was to determine which neural elements are excited by microstimulation of the CNS. The results demonstrate that near threshold the site of action potential initiation was always in the axon or the initial segment and did not occur in the soma. Furthermore, the site of excitation was a function of the electrode position, stimulus duration, and stimulus polarity. When the electrode was over the cell body, the site of action potential initiation could change with the amplitude of the stimulus current, and when the amplitude was much greater than threshold, initiation could occur in the cell body. When the excitation of two cells equidistant from the electrode was compared (one cell having the electrode over its cell body and the other having the electrode over a node of Ranvier), the cell that was excited depended on the stimulus duration. This result was robust to alterations in either the maximum membrane conductances or the intracellular resistivities of the model.

The neural element that experienced the largest amount of depolarization due to the stimulus was not always the site of action potential initiation. With the electrode in the region of the cell body, the cell body or dendrites experienced the greatest amount of depolarization, but action potential initiation occurred in the axon or initial segment (for both anodic and cathodic stimuli). The temporal evolution of the transmembrane potential played a strong role in determining the site of action potential initiation. These results (Figs. 2–4) indicate that the conclusion by Rattay (1998) that the activating function can predict the site of action potential initiation in CNS neurons may need revision. The influence of the electric field on the neuron, as predicted by the “activating function,” was not always an accurate indicator of the site of action potential initiation. Excitation was also dependent on the stimulus duration (Warman et al., 1992), and the response of the neuron was strongly dependent on the temporal evolution of the transmembrane potential during and after the stimulus pulse. Furthermore, these data suggest that the use of a passive model is not adequate to predict excitation of central neurons.

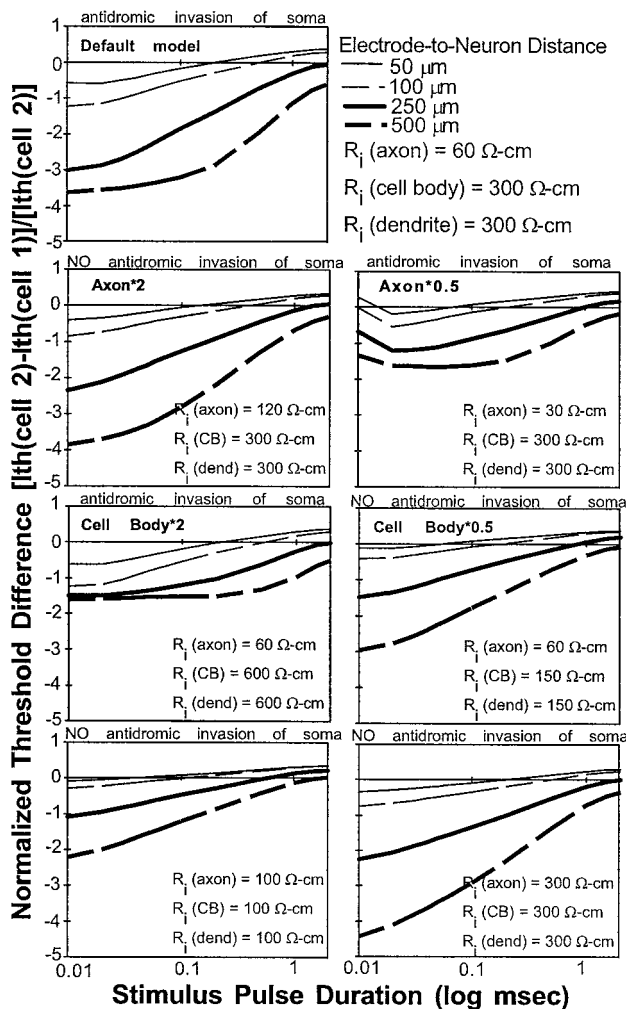


FIGURE 8 Sensitivity of the normalized threshold difference to changes in the intracellular resistivity values for the axon and cell body. Both the axoplasmic and cytoplasmic resistivities were doubled or halved individually. Two other model variants with equal intracellular resistivity values in each section of the model were also examined. The ability of each model variant to produce antidromic invasion of the soma is indicated above the respective plot.

Model limitations

This study of extracellular excitation of CNS neurons used a compartmental cable model with membrane dynamics and morphology representative of mammalian motoneurons. The model used in this study had four primary limitations. First, it used scaled Hodgkin-Huxley membrane dynamics to represent the nonlinear conductance properties of a cat spinal motoneuron. These scaled dynamics were an approximation of the actual mammalian neural properties, but the model was able to reproduce a wide range of experimental findings on motoneurons (see Model Reproduction of Experimental Data), and the sensitivity analysis showed the results of the model to be robust to alterations in these parameters.

Second, the model used a simplified geometry to represent the morphology of the dendritic tree. The model of the dendrite was equivalent to the full dendritic tree in terms of intracellular stimulation (Clements and Redman, 1989), but the membrane response generated by extracellular stimulation is dependent on the three-dimensional structure of the neuron. However, the dendrites in this model were passive and therefore only played a minor role in action potential initiation in the active sections of the cell body and axon.

Third, the model did not include the three-dimensional extent of the cell body, which may experience different extracellular potentials at different locations. For example, with the electrode positioned directly over the soma (diameter of 60 μm) at a distance of 50 μm (to the center), the potential difference from the top of the structure to the bottom was 233 mV for a threshold stimulus with a duration of 0.1 ms. To examine the effects of a distributed soma, a model was created with a 3-D representation of the cell body consisting of six instead of three compartments (maintaining the soma membrane surface area constant). The results of the 3-D model corresponded closely to the simplified 2-D model, with only a 5–10% increase in the relative threshold value for electrodes positioned over the soma. All of the conclusions from the 2-D model remained consistent with those of the 3-D model. These results suggest that the distributed nature of the soma plays a minor role in determining the site of action potential initiation.

Finally, the extracellular medium used in this study was isotropic and homogeneous. The extracellular medium of the CNS is anisotropic and inhomogeneous, and this can have an effect on extracellular excitation patterns. Differences in orientation between neurons in anisotropic media and inhomogeneities in the extracellular conductivity lead to alterations in the site of excitation (Grill, 1996). Given these limitations of the model, it was still able to reproduce experimentally documented characteristics of extracellular stimulation of central neurons.

Model reproduction of experimental data

The threshold profiles shown in Fig. 2 demonstrate that the position of the electrode with respect to the individual

neural elements had a large effect on the stimulus required to generate a propagating action potential. The sinusoidal shape of the threshold profile over the myelinated axon has been documented in experimental studies (BeMent and Ranck, 1969a; Roberts and Smith, 1973). The mean of the ratio between anodal and cathodal threshold currents for central fibers measured by BeMent and Ranck (1969a) was 4.57, which corresponds well to the model ratio of 5.25. The threshold profile near the cell body showed that for cathodic stimuli, electrode positions over the initial segment had the lowest thresholds, and thereafter the threshold increased with increasing longitudinal distance from the soma. This same pattern has been found in single-cell mapping studies of extracellular stimulation of spinal motoneurons (Gustafsson and Jankowska, 1976).

The model predictions of cathodic action potential initiation and propagation from extracellular stimuli (Figs. 3 and 5) also compare favorably with experimental data. The prediction of action potential initiation in axon nodes closest to the soma with the electrode over the cell body matches well with recent experimental studies in which extracellular stimulation initiated action potentials in the axons but not the cell bodies of rat cortical neurons (Norwak and Bullier, 1998a,b). This result can be explained by the effects of the extracellular field on the activation and inactivation gates of the sodium channel. A stimulus pulse applied over the cell body caused the cell body to be depolarized and the nodes near the cell body to be hyperpolarized (Fig. 3). This resulted in a removal of sodium inactivation at the nodes. Upon termination of the stimulus, the slow time constant of inactivation prevented recovery of inactivation, the node became hyperexcitable, and an action potential was initiated at the axon node rather than the cell body.

Nonpropagating orthodromic responses were produced when an antidromic action potential reached the cell body (Figs. 3 and 4). This behavior has also been documented experimentally, but the latencies of the initial segment (0.68 ms) and soma (1.33 ms) responses were slightly longer in the model than in experimental results (initial segment = 0.15–0.5 ms; somatodendritic = 0.2–1.0 ms) (Gogan et al., 1983; Gustafsson and Jankowska, 1976). The latencies of the initial segment and soma responses could be matched to the experimental measurements by decreasing the internodal distance of the first four internodes to 500 μm , a change consistent with recent anatomical data (Fabricius et al., 1994).

The CDR of the neuron was strongly dependent on the electrode position relative to the neuron. The slope of the CDR was much steeper for the electrode positioned over the cell body than for the electrode positioned over the axon (Fig. 5). Furthermore, the model results demonstrate that the site of action potential initiation changed as the electrode-to-neuron distance increased, and this contributed to the nonlinear shape of the CDR. Experimental data have shown that axons and cell bodies have CDRs with characteristics similar to those exhibited by the model (Ranck, 1975). Both experimental data and the model results show that with the

electrode positioned over the cell body, nonlinear CDRs are generated with slopes that are greater than when the electrode was positioned over the axon (Gustafsson and Jankowska, 1976). There are contrasting views on whether the CDRs of myelinated axons are linear or nonlinear over the range of electrode-to-neuron distances examined in this study. The model showed the CDR for the axon to be linear, which is consistent with experimental data from spinocerebellar tract fibers (Roberts and Smith, 1973). Other experimental studies have reported nonlinear relationships even for small ($<200 \mu\text{m}$) electrode-to-neuron distances (Jankowska and Roberts, 1972), whereas theoretical studies predict that the CDRs are linear at short distances and become nonlinear as the distance increases ($>600 \mu\text{m}$) (BeMent and Ranck, 1969b; Bean, 1974; Bean and King, 1976).

The model developed in this study was capable of reproducing a wide variety of experimental excitation patterns, but the extracellular currents needed for excitation were approximately an order of magnitude larger than those measured experimentally. In the microstimulation experiments reviewed by Ranck (1975), the levels of stimulation needed for excitation of both axons and cell bodies for electrode-to-neuron distances of $50\text{--}500 \mu\text{m}$ was in the range of $0.5\text{--}200 \mu\text{A}$ for stimulus pulse durations of $200 \mu\text{s}$. The model produced a range of $20\text{--}600 \mu\text{A}$ for the same stimulus pulse duration. The primary factor that contributed to this discrepancy was the difference in temperature between the model and experimental results. The temperature of the simulations run in the model was set to 20°C rather than 37°C , the approximate temperature in the microstimulation experiments. Temperature affects the conductance properties of the neuron, making it less excitable at lower temperatures (Schwarz and Eikhof, 1987). Another factor that may have contributed to the difference in the threshold currents was differences in the conductivity of the extracellular medium in the model and experiments (Grill, 1996).

Differential activation of nerve cells

The work of Gustafsson and Jankowska (1976) showed that the threshold for direct activation of nerve cells (cell bodies/initial segments) was similar to that for activation of nerve fibers. Furthermore, the consensus from the microstimulation experiments is that for cathodic stimuli cell bodies can be stimulated at lower current amplitudes than axons with long stimulus pulses, but under most conditions the axon will be much more excitable (Ranck, 1975). The results from this study support both of these conclusions (Figs. 2 and 6). The transitions from the activation of cell 2 (axon) to the activation of cell 1 (cell body) found in Fig. 6 can be explained by the differences in the strength-duration properties of the axon and the cell body. The point where one of the lines in Fig. 6 crosses 0 corresponds to a point where the strength-duration (S-D) relationships of the cell body and node cross (Fig. 9). The chronaxie (Tch) with the electrode

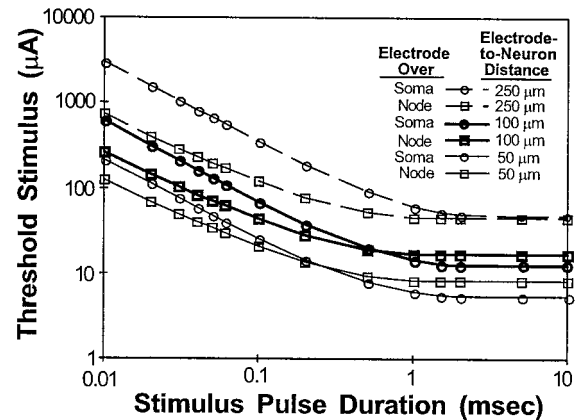


FIGURE 9 Strength-duration relationships for the electrode over an axon node far from the cell body and for the electrode over the soma at three different electrode-to-neuron distances.

over the cell body was nearly twice that with the electrode over the node at small electrode-to-neuron distances ($50 \mu\text{m}$), and this ratio increased to more than 3 at larger electrode-to-neuron distances ($500 \mu\text{m}$). This difference in the S-D relationships is supported by experimental results indicating that myelinated fibers have Tch values of $50\text{--}200 \mu\text{s}$ and cell bodies have Tch values of $200\text{--}700 \mu\text{s}$ (Ranck, 1975; Norwak and Bullier, 1998a). At short stimulus pulse durations the axon was excited with less current, but for long stimulus pulse durations the S-D curves of the node and cell body crossed, because of the difference in the chronaxies; the cell body, in turn, had a lower threshold (Fig. 9). Therefore, the pattern of activation was dependent on the selection of stimulus pulse duration.

CONCLUSION

The model of excitation of CNS neurons by extracellular sources used in this study was able to reproduce a wide range of experimental data, including the threshold profiles, current-distance, and strength-duration relationship data. Therefore, the model could be used to make inferences about the site of action potential initiation with a given electrode position and stimulus parameters, and the activation of one neuron relative to another. It was found that the site of action potential initiation with the electrode in the area of the cell body occurred in the axon or initial segment for a threshold stimulus. With cathodic stimuli at small electrode-to-neuron distances, the site of action potential initiation was dependent on the stimulus duration and the electrode-to-neuron distance. Short pulse durations produced lower thresholds for electrode positions over the axon, whereas longer pulse durations produced lower thresholds for electrodes positioned over the cell body. The site of excitation was also dependent on the polarity of the stimulus, with cathodic stimuli resulting in lower thresholds for electrode positions over the axon and anodic stimuli resulting in lower thresholds for electrode positions over the

cell body and dendrites. Furthermore, the site of maximum depolarization was not always the site of action potential initiation, and the temporal evolution of the membrane potential played a strong role in determining the site of action potential initiation.

The authors thank Dr. Michael Hines for helpful information in the use of NEURON and for a template for the threshold subroutine.

This work was supported by the National Science Foundation Biomedical Engineering and Research to Aid Persons with Disabilities Program (BES-9709488) and by the National Institutes of Health—National Institute of Neurological Disorders and Stroke Neural Prosthesis Program (N01-NS-5-2331).

REFERENCES

- Barrett, J. N., and W. E. Crill. 1974. Specific membrane properties of cat motoneurons. *J. Physiol. (Lond.)* 239:301–324.
- Bean, C. P. 1974. A theory of microstimulation of myelinated fibers. *J. Physiol. (Lond.)* 243:514–522.
- Bean, C. P., and R. J. King. 1976. Electrical microstimulation of smooth fibers. *Biophys. J.* 16:172a.
- BeMent, S. L., and J. B. Ranck. 1969a. A quantitative study of electrical stimulation of central myelinated fibers. *Exp. Neurol.* 24:147–170.
- BeMent, S. L., and J. B. Ranck. 1969b. A model for electrical stimulation of central myelinated fibers with monopolar electrodes. *Exp. Neurol.* 24:171–186.
- Clements, J. D., and S. J. Redman. 1989. Cable properties of cat spinal motoneurons measured by combining voltage clamp, current clamp and intracellular staining. *J. Physiol. (Lond.)* 409:63–87.
- Colbert, C. M., and D. Johnson. 1996. Axonal action-potential initiation and Na⁺ channel densities in the soma and axon initial segment of subicular pyramidal neurons. *J. Neurosci.* 16:6676–6686.
- Cullheim, S., J. W. Fleshman, W. W. Glenn, and R. E. Burke. 1987. Membrane area and dendritic structure in type-identified triceps surae alpha motoneurons. *J. Comp. Neurol.* 255:68–81.
- Cullheim, S., and J. O. Kellerth. 1978. A morphological study of the axon and recurrent axon collaterals of cat sciatic α -motoneurons after intracellular staining with horseradish peroxidase. *J. Comp. Neurol.* 178:537–558.
- Fabricius, C., C. H. Berthold, and M. Rydmark. 1994. Dimensions of individual alpha and gamma motor fibers in the ventral funiculus of the cat spinal cord. *J. Anat.* 184:319–333.
- Fleshman, J. W., I. Segev, and R. E. Burke. 1988. Electrotonic architecture of type-identified α -motoneurons in the cat spinal cord. *J. Neurophysiol.* 60:60–85.
- Gogan, P., J. P. Gueritaud, and S. Tyc-Dumont. 1983. Comparison of antidromic and orthodromic action potentials of identified motor axons in the cat's brain stem. *J. Physiol. (Lond.)* 335:205–220.
- Grill, W. M. 1996. Effects of tissue electrical properties on neural excitation. *Proc. 18th Annu. Int. Conf. IEEE-EMBS.* 2.2.2–6.
- Gustafsson, B., and E. Jankowska. 1976. Direct and indirect activation of nerve cells by electrical pulses applied extracellularly. *J. Physiol. (Lond.)* 258:33–61.
- Hille, B. 1992. *Ion Channels of Excitable Membranes*. Sinauer Associates, Sunderland, MA.
- Hines, M. L. 1993. NEURON—a program for simulation of nerve equations. In *Neural Systems: Analysis and Modeling*. J. Skrzypek, editor. Kluwer Academic Publishers, Norwell, MA. 127–136.
- Hines, M. L., and N. T. Carnevale. 1997. The NEURON simulation environment. *Neural Computation.* 9:1179–1209.
- Hines, M., and J. Moore. 1991. MH5.NRN a NEURON program: parameters and shapes to fit experimental observation of a cat spinal motoneuron. <http://www.neuro.duke.edu/demo/style.html>.
- Hodgkin, A. L., and A. F. Huxley. 1952. A quantitative description of membrane current and its application to conduction and excitation of nerve. *J. Physiol. (Lond.)* 117:500–544.
- Jankowska, E., and W. J. Roberts. 1972. An electrophysiological demonstration of the axonal projections of single spinal interneurons in the cat. *J. Physiol. (Lond.)* 222:597–622.
- Kellerth, J., C. Berthold, and S. Conradi. 1979. Electron microscopic studies of serially sectioned cat spinal α -motoneurons. III. Motoneurons innervating fast-twitch (type FF) units of the gastrocnemius muscle. *J. Comp. Neurol.* 184:755–768.
- Mainen, Z. F., J. Joerges, J. R. Huguenard, and T. J. Sejnowski. 1995. A model of spike initiation in neocortical pyramidal neurons. *Neuron.* 15:1427–1439.
- McIntyre, C. C., and W. M. Grill. 1997. Microstimulation of spinal motoneurons: a model study. *Proc. 19th Annu. Int. Conf. IEEE-EMBS.* 2032–2034.
- Norwak, L. G., and J. Bullier. 1998a. Axons, but not cell bodies, are activated by electrical stimulation in cortical gray matter. I. Evidence from chronaxie measurements. *Exp. Brain Res.* 118:477–488.
- Norwak, L. G., and J. Bullier. 1998b. Axons, but not cell bodies, are activated by electrical stimulation in cortical gray matter. II. Evidence from selective inactivation of cell bodies and axon initial segments. *Exp. Brain Res.* 118:489–500.
- Rall, W. 1977. Core conductor theory and cable properties of neurons. In *Handbook of Physiology: The Nervous System*. Vol. I. Cellular Biology of Neurons, Part I. E. R. Kandel, editor. American Physiology Society, Washington, DC. 39–97.
- Rall, W., R. E. Burke, W. R. Holmes, J. J. B. Jack, S. J. Redman, and I. Segev. 1992. Matching dendrite neuron models to experimental data. *Physiol. Rev.* 72:S159–S186.
- Ranck, J. B. 1975. Which elements are excited in electrical stimulation of mammalian central nervous system: a review. *Brain Res.* 98:417–440.
- Rattay, F. 1998. Analysis of the electrical excitation of CNS neurons. *IEEE Trans. Biomed. Eng.* 45:766–772.
- Roberts, W., and D. Smith. 1973. Analysis of threshold currents during microstimulation of fibers in the spinal cord. *Acta. Physiol. Scand.* 89:384–394.
- Schwarz, J. R., and G. Eikhof. 1987. Na currents and action potentials in rat myelinated nerve fibers at 20 and 37 degrees C. *Pflugers Arch.* 409:569–577.
- Schwindt, P., and W. Crill. 1984. Membrane properties of cat spinal motoneurons. In *Handbook of the Spinal Cord*. Vols. 2 and 3. Anatomy and Physiology. R. H. Dairdoff, editor. Marcel Dekker, New York.
- Segev, I., J. W. Fleshman, J. P. Miller, and B. Bunow. 1985. Modeling the electrical behavior of anatomically complex neurons using a network analysis program: passive membrane. *Biol. Cybern.* 53:27–40.
- Stephanova, D. I., and H. Bostock. 1995. A distributed-parameter model of the myelinated human motor nerve fiber: temporal and spatial distributions of electrotonic potentials and ionic currents. *Biol. Cybern.* 74:543–547.
- Tasaki, I. 1955. New measurements on the capacity and resistance of the myelin sheath and the nodal membrane of the isolated nerve fiber. *Am. J. Physiol.* 181:639–650.
- Thurbon, D., H. R. Lusche, T. Hofstetter, and S. J. Redman. 1998. Passive electrical properties of ventral horn neurons in rat spinal cord slices. *J. Neurophysiol.* 79:2485–2502.
- Tranchina, D., and C. Nicholson. 1986. A model for the polarization of neurons by extrinsically applied electric fields. *Biophys. J.* 50:1139–1156.
- Traub, R. D., J. G. R. Jefferys, R. Miles, M. A. Whittington, and K. Toth. 1994. A branching model of a rodent CA3 pyramidal neurone. *J. Physiol. (Lond.)* 481:79–95.
- Warman, E. N., W. M. Grill, and D. Durand. 1992. Modeling the effects of electric fields on nerve fibers: determination of excitation thresholds. *IEEE Trans. Biomed. Eng.* 39:1244–1254.